

# Minor- and Trace Element Zoning in Plagioclase From Kizimen Volcano, Kamchatka: Insights on the Magma Chamber Processes

Tatiana Churikova<sup>1,2</sup>, Gerhard Wörner<sup>2</sup>, John Eichelberger<sup>3</sup>, and Boris Ivanov<sup>1</sup>

Major and trace elements in whole rocks as well as major (Al, Si, Na, Ca, K), minor (Fe) and trace (Sr, Ba, Mg) elements in plagioclase phenocrysts were investigated in lavas from Kizimen volcano, Kamchatka. Quaternary Kizimen volcano was active during Holocene times and is intriguing in several aspects: (1) its lavas often contain unusually high proportions of incorporated basalt and basaltic andesite magma as enclaves; (2) banded texture is common in lavas; (3) large phenocrysts of plagioclase and hornblende associate with olivine and orthopyroxene in the same sample; (4) mafic enclaves and evolved dacites show a REE cross-over patterns; (5) MORB-like Sr-Nd isotope values exclude crustal contamination. Mafic enclaves and host dacitic lavas are both hybrid and represented by mixtures of mafic and silicic end-members in different proportions. These end-members are likely derivatives of the same basaltic parent assuming a significant amount of amphibole fractionation. To understand magma chamber processes of the Kizimen volcano and the origin of its magmas, we used major and trace element zoning patterns in plagioclase phenocrysts from mafic enclaves and evolved hosts. According to our data, mafic and silicic magmas maintain some identity as physically distinct domains, while sometimes exchanging only heat but at other times heat, melt, and crystals between them. Processes in the magma chamber that occurred before eruption are: (1) crystal growth and fractionation, (2) recharge and magma mixing, and (3) resumed crystallization in high-temperature dacite heated by mafic magma.

## 1. INTRODUCTION

Magma chamber processes play an important role in the formation of igneous rocks. These processes include crys-

tallization, melt differentiation, convection, and magma mixing. Experimental and numerical models of magma chamber processes [e.g. *Marsh*, 1989] allow study of the effects of physical parameters such as density and viscosity as a function of melt composition, temperature gradients inside the chamber and near the contact with country rock, geometry of the magma chamber, etc. However, such models need to be calibrated with natural systems, and it is difficult to apply them directly because many of these parameters are not well constrained.

One approach to better understand mixing dynamics in magmas is the study of the crystallization histories of minerals in volcanic rocks, using major, minor, and trace element zoning in plagioclase in relation to magma

<sup>1</sup> Institute of Volcanology and Seismology Far East Division Russian Academy of Sciences, Kamchatka, Russia

<sup>2</sup> Geowissenschaftliches Zentrum Göttingen, Universität Göttingen, Germany

<sup>3</sup> Alaska Volcano Observatory, Geophysical Institute, University of Alaska Fairbanks, Fairbanks, Alaska, USA

Volcanism and Subduction: The Kamchatka Region  
Geophysical Monograph Series 172

Copyright 2007 by the American Geophysical Union.  
10.1029/172GM22

compositions and crystallization conditions. Plagioclase is the best mineral for such kind of research because it faithfully records the changes in magma compositions at variable temporal and spatial scales without significant subsequent re-equilibration [Grove *et al.* 1981, Davidson and Tepley, 1997; Ginibre *et al.*, 2002a, 2002b]. However, controls on its composition are also rather complex and difficult to separate. Numerical modeling [e.g. Allègre *et al.*, 1981] has provided insights into the kinetics of plagioclase growth and resorption. Experimental studies have elucidated the influence of some important factors (e.g. P, T, melt composition, H<sub>2</sub>O content in the melt) on the An–Ab system (e.g. Drake and Weill, 1975; Bindeman *et al.*, 1998).

Recently, significant variations in minor, trace elements and isotope ratios between individual growth zones of natural plagioclase crystals at the scale of several microns were revealed using SIMS and TIMS techniques [Churikova and Sokolov, 1993; Brophy *et al.*, 1996; Davidson and Tepley 1997; Tepley *et al.*, 2000]. These variations have been attributed to processes occurring during magma storage and ascent, including fractional crystallization, magma mixing, degassing, assimilation, and temperature effects. The spatial resolution of the SIMS and TIMS is insufficient to reveal chemical variations in individual growth zones at a micron scale. The electron microprobe allows to measure the major, minor and trace elements (if concentrations > 100 ppm) in minerals with a spatial resolution of only a few microns [e.g. Ginibre *et al.*, 2002a, b]. Such an approach allows studying a greater number of crystals at higher spatial resolution and at significantly lower cost.

In this study we report the results of microprobe analyses on plagioclase phenocrysts from basalts, basaltic andesites and dacites of Kizimen volcano (Kamchatka, Figure 1). Tephrochronological work on the eruption history of Kizimen has shown that the volcano formed during the Quaternary [Melekestsev *et al.*, 1992] synchronously with an associated graben and was active until Late Holocene time. Its structural setting, and indeed its morphology and petrology, is strikingly similar to Unzen Volcano in Japan [Nakada & Motomura, 1999; Browne *et al.*, 2006]. At present, there is intense fumarolic activity on the slope of the volcano.

Our geochemical investigation of Kizimen volcano was conducted in several stages. First, we analyzed the major and trace elements as well as isotope ratios of Sr, Nd (in three samples) and Pb (in one sample) in whole rocks. Then we studied six plagioclase phenocrysts from three representative samples for major (Al, Si, Na, Ca, K), minor (Fe) and trace (Sr, Ba, Mg) elements.

## 2. GEOLOGICAL SETTING, PETROGRAPHY AND MINERALOGY OF SAMPLES STUDIED

Kizimen Volcano, one of the active volcanoes of the Kurile-Kamchatka arc, is located on the eastern margin of the Central Kamchatka Depression (CKD) in the area of Schapinsky graben midway between the Eastern Volcanic Front (EVF) and CKD at the latitude of the Kliuchevskaya Group (Figure 1). The northwestern part of the volcano is cut by NE-SW-trending, westward-dipping normal faults, which form a series of cliffs with good exposures of the volcano's flank and its basement. A single reported eruption, in 1928, was very modest and no deposits were found.

Four cycles of activity have been identified in the eruptive history of the volcano (Figure 1), with ages from 12–11 Ka to present [Melekestsev *et al.*, 1992]. Holocene eruptions produced lava flows and a dome complex of basaltic andesite to dacite composition in the upper part of volcano (Figure 1). Andesite and dacite lava flows contain abundant cognate mafic enclaves of more primitive composition (Figure 2a). The most recent summit lava has an unusual high proportion of up to 35 vol % of large (> 20 cm) mafic enclaves of basaltic andesite composition. Dacitic lavas with a few percent of enclaves of smaller size are more common (Figure 2b). We did not find any correlations between shape of enclaves and their composition. There are also abundant conspicuously banded lavas, with an apparent thickness of mafic layers from a few millimeters to 20–25 cm (Figure 2c) thick. All andesite to dacite lavas are hornblende-bearing medium-potassic, and calc-alkaline in composition (Figure 3), and the enclaves are basaltic to basaltic andesites [Churikova *et al.*, 2001b].

All samples from basalts to dacites contain plagioclase, hornblende, orthopyroxene, olivine, Ti-magnetite and glass. The amount of olivine decreases from 5 vol% in basalts to a trace in dacite. Basalts are also richer in orthopyroxene compared to dacites, 20 vol% and 10 vol%, respectively. In contrast, the amount of hornblende increases from 5 vol% in basaltic enclaves to 10–15 vol% in andesites and dacites. The amount of plagioclase and Ti-magnetite is rather similar in all rocks, about 20–25 vol% and 2–3 vol%, respectively. Additionally, basalts and basaltic andesites have about 5% of high-Ca clinopyroxene, whereas dacites often contain 0.5–1 vol% quartz [Trusov & Pletchov, 2005].

The composition of minerals in all types of rocks is surprisingly similar: Fo<sub>79-72</sub> olivine, En<sub>63-65</sub>Wo<sub>1-2</sub> orthopyroxene, titanomagnetite, and high-Mg amphibole. Only plagioclases show conspicuous compositional variations.

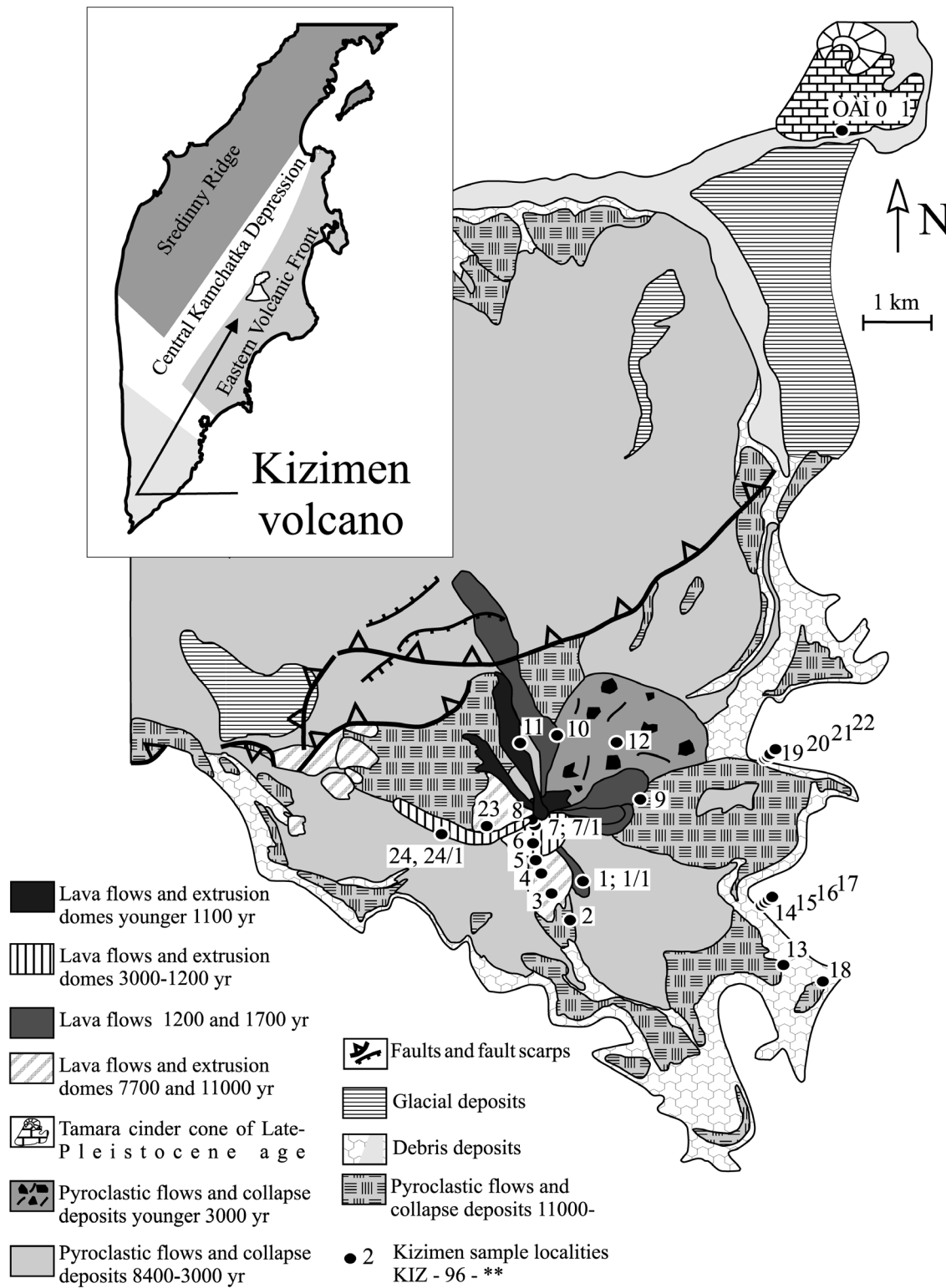


**Figure 1.** Schematic map of the Kizimen volcano and its surroundings [after *Melekestsev et al.*, 1992]. Inset shows the location of Kizimen volcano at the border between Eastern Volcanic Front and Central Kamchatka Depression. All ages are in B.P.

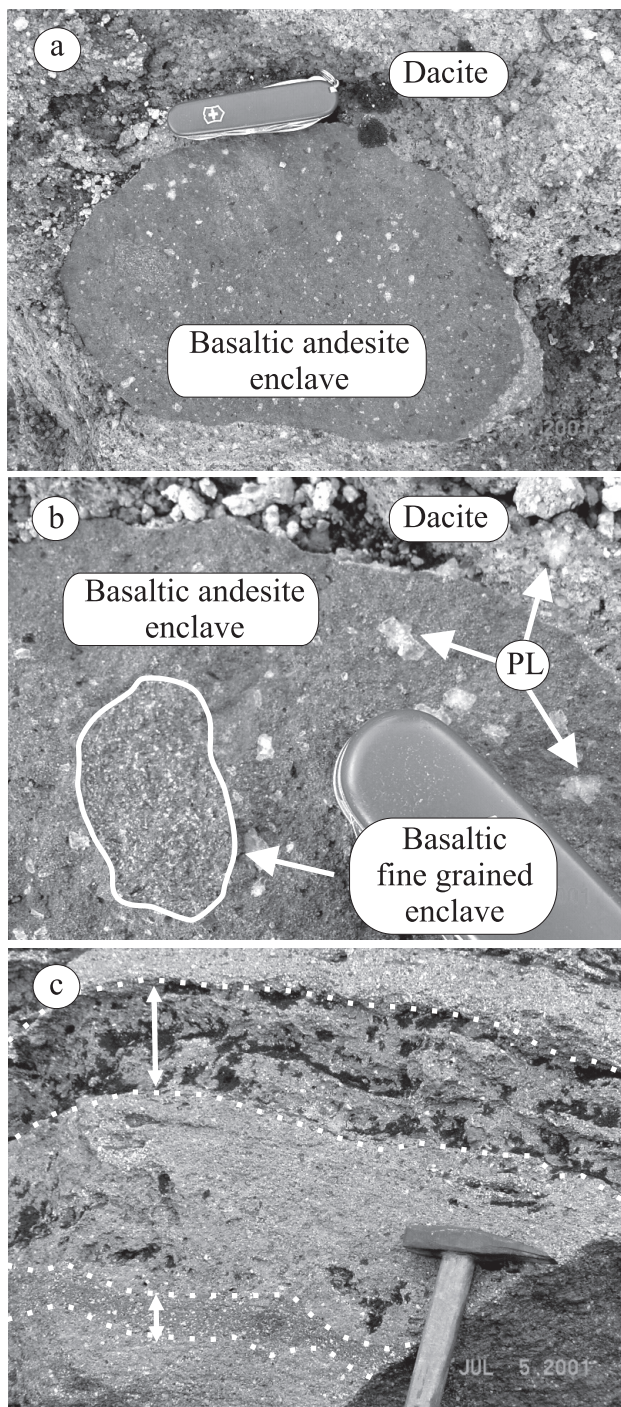


**Figure 2.** (a) Large basaltic andesite enclave (17\*20 cm) in a dacitic lava; (b) 5-cm-diameter fine-grained enclave of basaltic composition inside a larger basaltic andesite enclave in dacitic host. Plagioclase crystals of more than 1 cm in size are found in both, host dacite and mafic enclave (shown by arrows); (c) fragment of the banded lava, the thickness of the layers is shown by double arrows.

In our view, the most prominent characteristic of Kizimen rocks is the occurrence of large phenocrysts of plagioclase and hornblende (up to 2 cm) co-existing with olivine and orthopyroxene.

### 3. ANALYTICAL METHODS

Analyzes were performed in Geowissenschaftliches Zentrum of Göttingen Georg-August Universität, Abteilung Geochemie, Germany. Major elements and some trace elements (Sc, V, Cr, Co, Ni, Zn, Ga, Rb, Sr, Zr, and Ba) were determined in 19 samples by X-ray fluorescence analysis on glass discs, prepared with a lithium tetraborate flux.  $\text{Fe}_2\text{O}_3$  was determined titrimetrically with  $\text{KMnO}_5$  and the loss on ignition (LOI) by weight difference at heating to  $1100^\circ\text{C}$ . The analytical uncertainty ( $\pm 2\sigma$ , rel. %) for all major elements is better than 1 % except for Fe, Na (2%) and LOI (10%), whereas for trace elements it is better than 5 %.

Additional trace elements were analyzed in 7 samples by ICPMS. The analytical uncertainty for most elements was better than 10 rel. %, except for Nb and Ta (15–20 rel. %), which was estimated based on repeated analyses of rock standards JB-3 and JA-2.

Isotope ratios for Sr, Nd, and Pb were measured with a Finnigan MAT 262 RPQ II+ mass-spectrometer at Göttingen using standards NBS987 (0.710245) for Sr, LaJolla (0.511847) for Nd and NBS981 (recommended values from *Todt et al.*, 1984) for Pb. Statistical errors ( $\pm 2\sigma$ ) were estimated to be less than 0.004% for Sr and Nd and less than 0.1% for Pb. For details see Dorendorf et al. [2000a, b] and Churikova et al. [2001a].

Major (Si, Al, Ca, Na, and K), minor (Fe) and trace (Sr, Mg, Ba) elements in six plagioclase grains were analyzed using JEOL8900 electron microprobe. This study was combined with textural observations using back scattered electron (BSE) images (multiply accumulated to increase mass resolution) where BSE intensity corresponds to An content. The BSE images were used to locate quantitative measurement points along profiles from core to rim. The central parts and the rims of microlites in the same samples were also analyzed for comparison.

Details of the technique for major and trace element determination with electron microprobe JEOL8900 WDS were described in Ginibre et al. [2002a]. Microprobe quantitative point analyses for Al, Si, Na, Ca, K, Ba, Sr, Fe, Ti, Ba, Mg were performed at 20 kV acceleration voltage and 40 nA beam current, with 2 to 5  $\mu\text{m}$  beam size. Alkali elements (Na, K) and major elements (Al, Si, Ca) were analyzed during the first 90 s (16 s counting time on peak). Minor (Fe) and trace elements (Sr, Ba, Mg) were then analyzed over 4 min counting time on the peak.

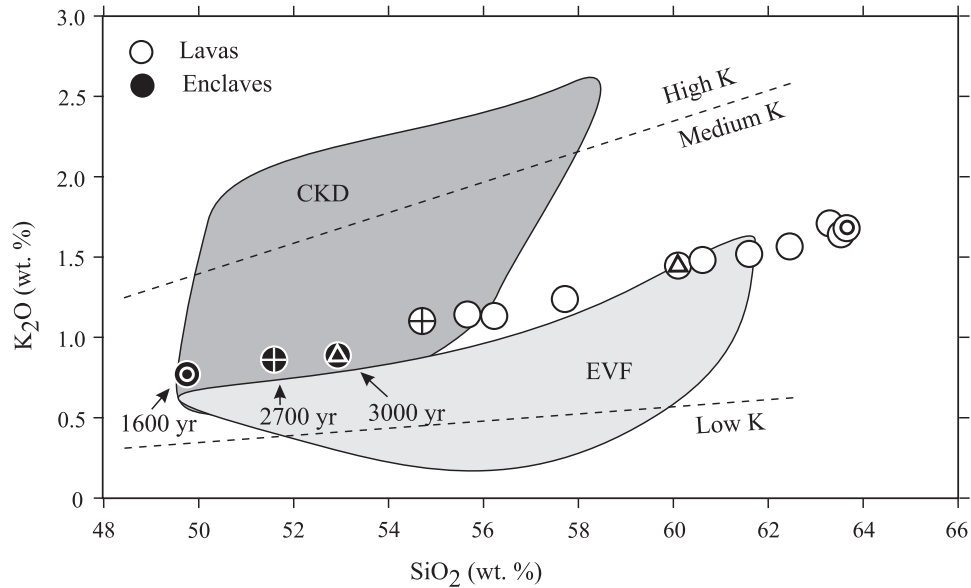


**Figure 3.**  $K_2O$  vs.  $SiO_2$  for Kizimen volcano whole rocks. Rock chemistry within the mafic enclaves changes with time towards more mafic compositions. Compositional fields of EVF and CKD are shown for the comparison [after Churikova *et al.*, 2001a]. The pairs of rocks (host rock – mafic enclave) for three eruptions are shown by additional symbols (crosses, circles and triangles). Ages are taken from Melekestsev *et al.* (1992) and given in B.P.

The detection limits for Ba, Sr, Fe, Mg, and Ti, as well as the ranges of concentrations and analytical uncertainties for the analyses at the concentrations measured are given in Ginibre *et al.* [2002b]. Typical analytical uncertainties calculated from counting statistics for each analysis were 19 ppm for Mg, 60–70 ppm for Fe, 110–120 ppm for Sr, 70–75 ppm for Ba and 28–31 ppm for Ti.

#### 4. RESULTS

##### 4.1. Whole-Rock Geochemical Data From Kizimen Volcano.

Lavas and mafic enclaves define linear trend in  $K_2O$  versus  $SiO_2$  compositional space (Figure 3). Enclaves in dacites become more mafic in more recent lavas. Kizimen lavas appeared to be transitional between the EVF and the CKD, i.e. they are more enriched in alkalis than the rocks of EVF but depleted in alkalis as compared to basalts and basaltic andesites of CKD (Figure 3). This is part of the systematic compositional trend from the Eastern Volcanic Front (EVF) through the Central Kamchatka Depression (CKD) to the back arc [Churikova *et al.*, 2001a].

Trace element patterns for products of the Kizimen volcano are typical for arc volcanism. They are characterized by strongly but variably enriched fluid mobile trace elements (LILE and LREE: K, Cs, U, Ba, Rb, Sr, Pb, La, and Ce) and relatively depleted HFSE (Nb, Ta, Hf, Zr, Ti) and

HREE (from Tb to Yb) elements. The enrichment increases with increasing element compatibility. Ba, Rb, U, Th, and K have more than 10 times higher concentrations compared to NMORB. However, the andesitic and dacitic lavas show a stronger gradient from the most incompatible to less incompatible elements than the basaltic and basaltic-andesitic enclaves (Figure 4). This results in a cross-over pattern because the HREE concentrations in dacitic rocks are lower than in basaltic rocks.

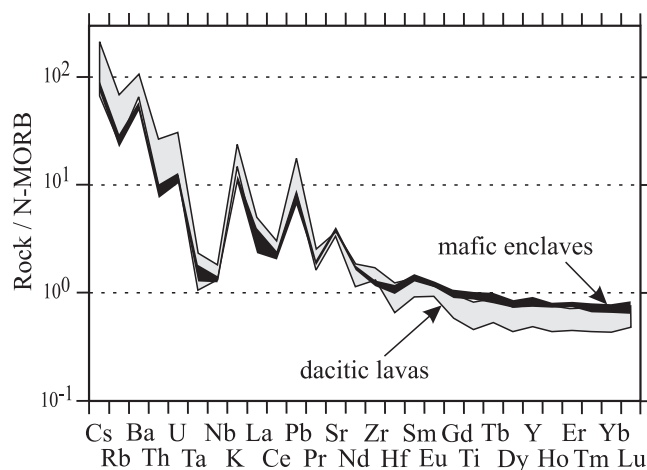


**Figure 4.** Trace element patterns for Kizimen lavas (gray field) and mafic enclaves (black field). All data are normalized to NMORB [after Sun & McDonough, 1989].

Sr- and Nd-isotope ratios for the three most mafic rocks are very close to each other ( $^{87}\text{Sr}/^{86}\text{Sr}$ : 0.703352 – 0.703370;  $^{143}\text{Nd}/^{144}\text{Nd}$ : 0.513045–0.513048). They fall within the range of Kamchatka rocks (i.e., where the fields for EVF, CKD and Sredinny Ridge of the back arc overlap; *Churikova et al.*, 2001a) and are close to the MORB-field.

Thus rocks of Kizimen volcano are represented by typical arc lavas of medium-K calc-alkaline series with strong but variable LILE and LREE enrichment and low HFSE. Mafic enclaves and evolved dacites show a REE cross-over patterns. In isotope space they are close to NMORB.

#### 4.2. Zoning Trends in Plagioclase Phenocrysts From Kizimen Volcano

We studied the plagioclase phenocrysts from host lavas and its enclaves in three samples: a) dacite lava from the one of the summit flows (KIZ-07; 60.10 wt%  $\text{SiO}_2$ ), b) a basaltic-andesite enclave in this lava flow (KIZ-07/1; 52.90 wt%  $\text{SiO}_2$ ), and c) a mafic enclave from a second summit flow (KIZ-01/1; 49.70 wt%  $\text{SiO}_2$ ; Table 1, Figure 1). All three samples were erupted during the current eruptive cycle [*Melekestsev et al.*, 1992], which began 3,000 years ago. Morphologically, three types of plagioclases were distinguished in all studied rocks.

Pl-1 occurs predominantly in mafic enclaves and less frequently in the host dacite. Pl-1 is characterized by euhedral shape and 20–50-micron-wide zones of growth (Figure 5a). The cores of these crystals sometimes have patchy textures (Figure 5a) or they are relatively homogeneous (not shown). Cores and mantles are compositionally uniform, whereas rims are characterized by steep compositional gradients.

Pl-2 crystals, found only in host dacitic lavas, show very narrow oscillatory zonation (5–50  $\mu\text{m}$ ) throughout. Pl-2 has usually numerous dissolution surfaces in the mantle zone, with subsequent regrowth (Figure 6a). The outermost zones are very narrow (5–10  $\mu\text{m}$ ).

Pl-3 crystals were observed in both mafic enclaves and in host dacite. It has subhedral to irregular shapes. Pl-3 crystals have continuous (from tens to first hundreds of microns) sieved zones. In some grains such zones make up more than 50% of the crystal. However, the outermost rims of these crystals are well formed and show clear contact with groundmass (Figures 5b, 6b). The cores of Pl-3 crystals show numerous narrow growth zones that are texturally similar to the Pl-2 phenocrysts from the dacitic lavas. We analyzed different zones in 2 grains of Pl-1, in 2 grains of Pl-2 and in 2 grains of Pl-3 (1 from enclave and 1 from host lava) for major (Al, Si, Na, Ca, K), minor (Fe) and trace (Sr, Ba, Mg) elements. Point measurements were taken along profiles from core to rim with spot size 2–5  $\mu\text{m}$  (Figures 5 and 6; Table 2).

*4.2.1. Pl-1 in mafic enclaves.* Pl-1 phenocrysts from basalt and basaltic andesite enclaves are characterized by the absence of any significant zoning in their cores (Figure 5a), which composition is the most calcic found in Kizimen rocks ( $\text{An}_{86}\text{-An}_{93}$ , see insert in Figure 5a). These cores sometimes have partly sieved texture (Figure 5a) and include hornblende and patches of more sodic plagioclase ( $\text{An}_{77}$ , see points 6 and 7 on the Figure 5a). The mantle zone between core and rim is close in composition to the core ( $\text{An}_{77}\text{-An}_{93}$ ). Cores and their mantles are low in Ba (< 50 ppm) and moderately high in Sr (300 – 550 ppm). Fe and Mg concentrations are high (up to 5000 ppm and 300 – 500 ppm, respectively).

Rims of Pl-1 are very different from the cores and mantle zones. The thickness of the outer rims varies from several microns to 100 microns. Composition of the rims is more sodic ( $\text{An}_{74\text{-}36}$ ) than the inner parts of the grains, and An content decreases outwards. Sr and Ba concentrations in the rim increase to 900 ppm and 500 ppm, respectively, whereas Fe and Mg decrease to 2800 ppm and 200 ppm, respectively (Figure 5a). Plagioclase microlites in the enclaves are similar in composition to rims of Pl-1.

*4.2.2. Pl-2 in dacitic lavas* are relatively large in size (up to 2 cm, Figures 2b, 6a) and characterized by narrow oscillatory zonation. In contrast to Pl-1 from the enclaves, the cores and mantle zones of Pl-2 are rather sodic ( $\text{An}_{40}\text{-An}_{50}$ ) and show higher Sr (500 – 750 ppm) and Ba (150–300 ppm) concentrations and lower Fe (1500–2000 ppm) and Mg (100–150 ppm). Because elemental concentrations change so strongly from one growth zone to another, the zoning patterns of Pl-2 are much more variable compared to the Pl-1 phenocrysts from the mafic enclaves (Figure 6a). The thickness of the outermost rims is less than 50 microns. The rims differ in chemical composition from the cores and mantle zones of the crystals. However, in contrast to Pl-1, the rims of Pl-2 are enriched in anorthite component, Fe, and Mg and depleted in Ba and Sr (Figures 6a, 7) compared to the core and mantle zones. Microlites of the dacitic host are similar in chemical composition to the rim of Pl-2.

*4.2.3. Pl-3 in dacitic lavas and mafic enclaves* are surprisingly similar in crystal morphology and chemical composition. Three distinct growth zones are present in these grains: (I) oscillatory-zoned, compositionally uniform inner core, (II) a sieve-textured zone with a thickness from 50 up to 200 microns and (III) about 50-micron-wide outermost rim (Figures 5b, 6b). Cores of Pl-3 phenocrysts are similar in composition to cores of Pl-2 phenocrysts from dacitic lavas. They are low in An, Fe, and Mg at relatively high concentrations of Ba and Sr. In the sieve-

**Table 1.** Chemical composition and isotope data for whole rocks of the Kizimen volcano.

Sample	TAM-01	KIZ-01	KIZ-01/1 <sup>b</sup>	KIZ-02	KIZ-04	KIZ-05	KIZ-07	KIZ-07/1	KIZ-08	KIZ-09
SiO <sub>2</sub>	51.75 <sup>a</sup>	64.11	50.23	62.63	62.14	57.10	60.43	53.28	58.13	63.88
TiO <sub>2</sub>	0.84	0.58	1.23	0.65	0.68	0.90	0.77	1.11	0.94	0.62
Al <sub>2</sub> O <sub>3</sub>	15.87	16.30	19.04	16.60	17.73	17.54	16.96	18.48	17.25	16.25
Fe <sub>2</sub> O <sub>3</sub>	9.43	2.43	5.38	2.70	2.82	3.48	3.85	4.25	3.66	2.43
FeO	0.43	3.05	5.62	3.22	2.59	4.83	3.11	5.34	4.22	3.13
MnO	0.19	0.13	0.19	0.14	0.13	0.17	0.15	0.19	0.17	0.13
MgO	8.49	2.46	5.26	2.68	2.72	4.05	3.12	4.44	3.61	2.43
CaO	9.29	5.38	9.35	5.91	5.77	7.28	6.38	8.54	7.12	5.47
Na <sub>2</sub> O	2.74	3.72	2.77	3.74	3.70	3.32	3.60	3.28	3.47	3.77
K <sub>2</sub> O	0.73	1.67	0.77	1.58	1.52	1.16	1.47	0.90	1.26	1.74
P <sub>2</sub> O <sub>5</sub>	0.23	0.16	0.17	0.15	0.19	0.16	0.16	0.19	0.18	0.15
Total	100	100	100	100	100	100	100	100	100	100
Li	7.9	16.3	14.2			10.2				
Be	0.51	0.79	0.52			0.63				
Sc	31	15	26	17	15	21	18	26	24	15
V	221	114	300	137	146	208	163	250	199	115
Cr	481	17	15	16	26	10	12	11	19	13
Co	36	14	30	18	14	29	17	26	21	13
Ni	166	n.d. <sup>c</sup>	2	n.d.	1	7	n.d.	n.d.	n.d.	n.d.
Zn	79	55	79	61	57	68	63	74	65	55
Ga	15	16	17	16	15	17	15	18	16	15
Rb	15	38	14	34*	32*	26	31*	17*	25*	41*
Sr	380	319	370	328	318	330	320	368	325	304
Y	16	16	21	19*	15*	20	22*	24*	22*	18*
Zr	86	121	86	124	115	102	117	96	117	126
Nb	2.4	4.2	2.9	5.0*	6.0*	3.5	4.0*	3.0*	4.0*	4.0*
Cs	0.50	1.50	0.52			0.47				
Ba	358	676	310	593	608	458	567	376	451	655
La	7.62	10.16	5.85			7.73				
Ce	19.02	22.39	15.18			19.37				
Pr	2.69	3.32	2.34			2.76				
Nd	13.10	13.54	11.99			12.79				
Sm	3.72	2.89	3.36			3.23				
Eu	1.11	0.95	1.14			1.04				
Gd	3.29	2.58	3.28			2.97				
Tb	0.52	0.36	0.54			0.44				
Dy	3.38	2.28	3.33			2.94				
Ho	0.67	0.55	0.74			0.65				
Er	2.06	1.46	2.18			1.85				
Tm	0.32	0.20	0.30			0.26				
Yb	2.05	1.39	2.00			1.72				
Lu	0.31	0.24	0.29			0.28				
Hf	2.27	1.91	1.99			1.88				
Ta	0.19	0.21	0.17			0.17				
Tl	0.03	0.27	0.10			0.10				
Pb	2.15	5.30	1.95			3.01				
Th	0.91	3.19	1.02			1.42				
U	0.45	1.45	0.49			0.79				
<sup>87</sup> Sr/ <sup>86</sup> Sr			0.703352							
<sup>143</sup> Nd/ <sup>144</sup> Nd			0.513045							
<sup>206</sup> Pb/ <sup>204</sup> Pb										
<sup>208</sup> Pb/ <sup>204</sup> Pb										
<sup>207</sup> Pb/ <sup>204</sup> Pb										

<sup>a</sup>Major elements, Sc, V, Cr, Co, Ni, Zn, Ga, Sr, Zr, Ba and elements marked by stars were determined by XRF analyses, other trace elements were achieved by ICP-MS. Major elements are given in weight percent, trace elements in ppm.

<sup>b</sup>Samples KIZ-01/1, KIZ-07/1 and KIZ-24/1 are mafic enclaves in lavas KIZ-01, KIZ-07 and KIZ-24, respectively.

<sup>c</sup>Not detected

**Table 1.** (continued).

Sample	KIZ-11	KIZ-17/2 <sup>d</sup>	KIZ-18	KIZ-19	KIZ-21	KIZ-22	KIZ-23	KIZ-24	KIZ-24/1
SiO <sub>2</sub>	56.07	57.72	62.30	51.53	56.72	62.40	64.26	55.43	52.28
TiO <sub>2</sub>	0.98	0.85	0.68	1.23	1.10	0.65	0.59	1.04	1.30
Al <sub>2</sub> O <sub>3</sub>	17.73	17.32	16.69	16.90	17.63	16.84	16.31	17.67	18.15
Fe <sub>2</sub> O <sub>3</sub>	2.92	2.78	2.49	3.04	3.21	3.14	2.63	3.11	4.35
FeO	5.56	4.88	3.56	8.21	5.08	2.96	2.77	5.56	5.86
MnO	0.17	0.17	0.14	0.22	0.18	0.13	0.13	0.17	0.19
MgO	4.19	4.17	2.75	5.35	3.12	2.91	2.39	4.22	4.48
CaO	7.75	7.29	5.91	9.82	7.54	5.81	5.37	8.29	9.25
Na <sub>2</sub> O	3.32	3.35	3.80	2.77	3.75	3.57	3.73	3.22	3.07
K <sub>2</sub> O	1.15	1.29	1.54	0.73	1.40	1.43	1.68	1.11	0.88
P <sub>2</sub> O <sub>5</sub>	0.17	0.18	0.15	0.22	0.27	0.16	0.15	0.17	0.19
Total	100	100	100	100	100	100	100	100	100
Li				3.8				8.5	11.7
Be				0.44				0.56	0.56
Sc	21	22	18	35	26	16	13	22	33
V	220	190	133	316	187	130	108	246	324
Cr	16	47	20	42	11	34	19	24	21
Co	27	20	21	37	20	14	13	27	27
Ni	6	20	1	25	n.d.	8	2	2	n.d.
Zn	71	76	58	94	83	60	57	72	80
Ga	16	17	16	18	19	15	15	19	17
Rb	24*	28*	33*	9	15*	30*	36*	21	16
Sr	332	359	324	276	299	341	320	328	335
Y	23*	24*	20*	32	34*	15*	19*	20	23
Zr	98	124	124	104	140	109	124	99	90
Nb	4.0*	4.0*	3.0*	4.1	6.0*	3.0*	4.0*	3.1	3.2
Cs				0.31				0.79	0.59
Ba	459	466	606	164	200	591	669	419	323
La				6.49				6.52	7.02
Ce				19.11				16.57	18.10
Pr				2.73				2.83	2.59
Nd				13.11				12.73	13.08
Sm				3.86				3.25	3.91
Eu				1.14				1.08	1.27
Gd				4.04				3.12	3.53
Tb				0.70				0.47	0.63
Dy				4.37				3.08	3.88
Ho				0.94				0.76	0.75
Er				2.89				1.97	2.23
Tm				0.42				0.27	0.34
Yb				2.77				1.72	2.38
Lu				0.42				0.30	0.32
Hf				2.80				2.10	2.17
Ta				0.21				0.14	0.19
Tl				0.05				0.09	0.10
Pb				2.03				2.73	2.63
Th				0.59				1.57	0.91
U				0.38				0.77	0.61
<sup>87</sup> Sr/ <sup>86</sup> Sr								0.703347	0.703370
<sup>143</sup> Nd/ <sup>144</sup> Nd								0.513048	0.513047
<sup>206</sup> Pb/ <sup>204</sup> Pb									18.32
<sup>208</sup> Pb/ <sup>204</sup> Pb									38.03
<sup>207</sup> Pb/ <sup>204</sup> Pb									15.50

<sup>d</sup>Samples KIZ-17/2, KIZ-19, KIZ-21 and KIZ-22 are from old volcano basement, other samples are Quaternary age.

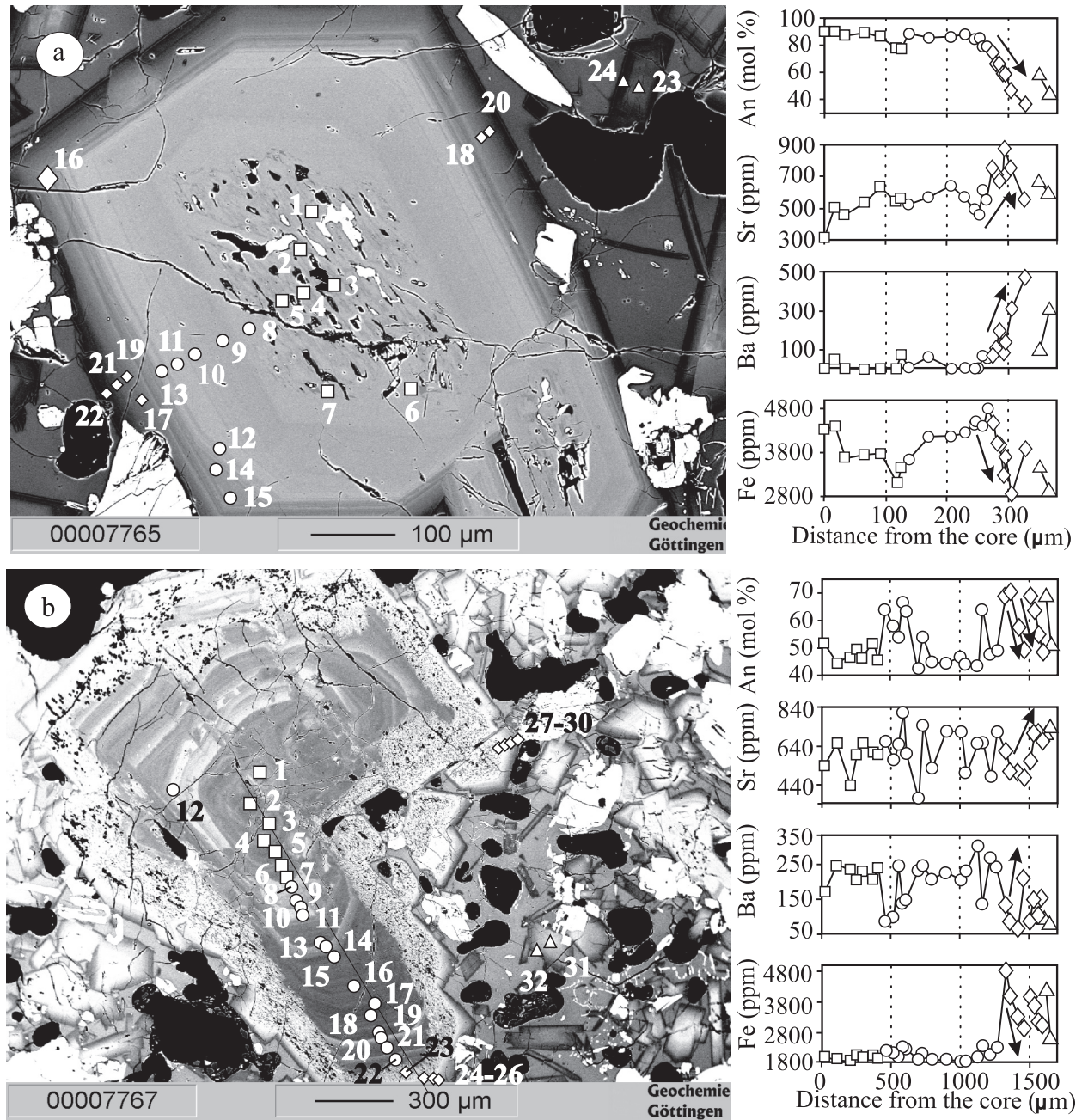


**Figure 5.** Electron microprobe traverses across plagioclase phenocrysts from a representative basaltic enclave. (a) un-resorbed plagioclase and (b) resorbed plagioclase. Compositional profiles are shown in mol. % for An content and in ppm for Sr, Ba, and Fe concentrations. The abrupt in chemical composition near the crystal margins is indicated by arrows. Squares are data from the crystal cores, circles from the mantle, diamonds represent the rim and triangles are for microlites.

textured zone the plagioclase composition becomes more calcic up to An<sub>80</sub>, whereas concentrations of Fe and Mg increase up to 5000 ppm and 550 ppm, respectively, and Sr and Ba values decrease. The rim zone Pl-3 is more sodic

than the sieve-textured zone, but not quite as Ab-rich as the core. Microlites near Pl-2 phenocrysts are similar in chemical composition to zones II and III of Pl-3 (inset Figures 5b, 6b).

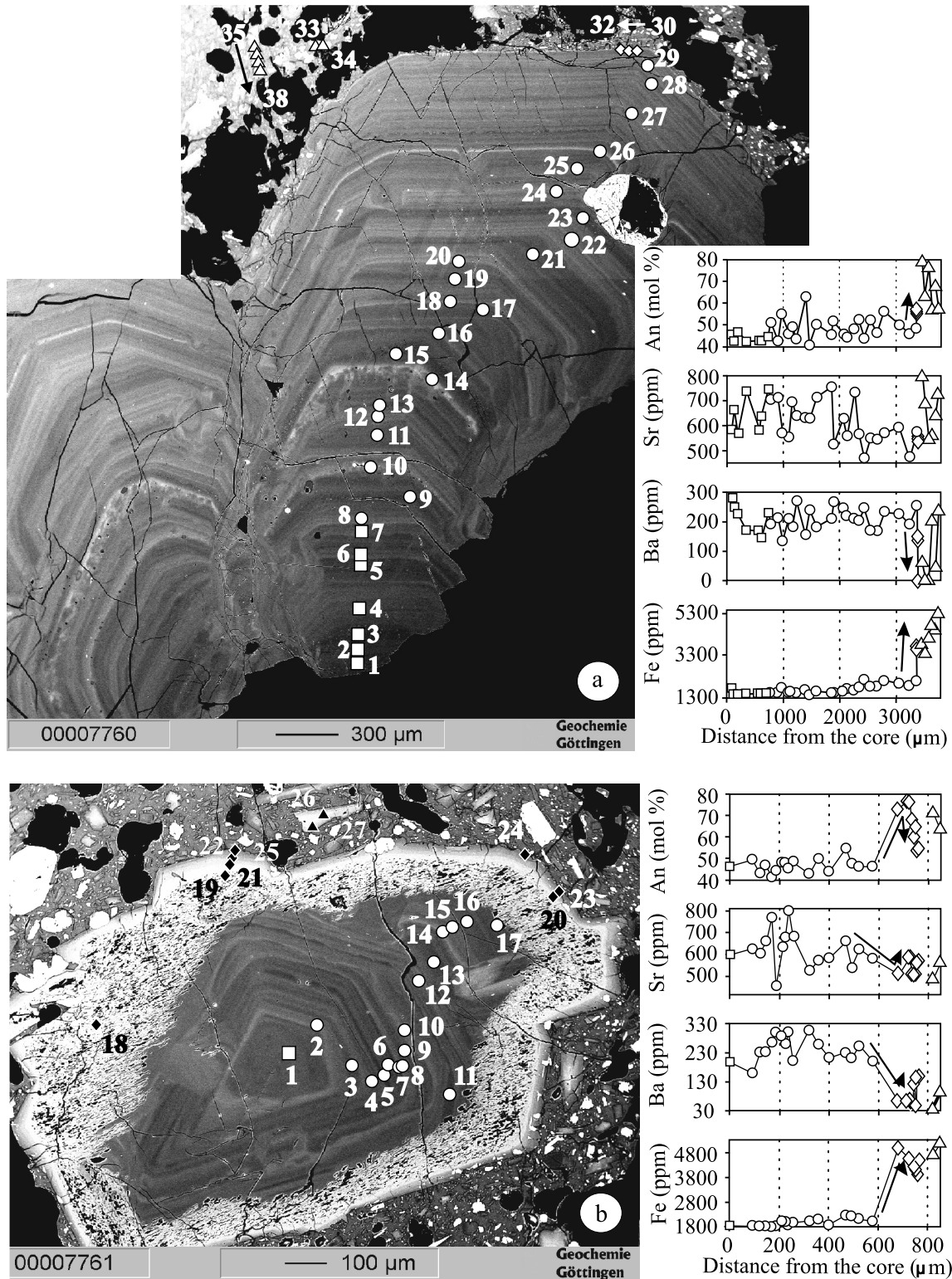


**Figure 6.** Electron microprobe traverses across plagioclase phenocrysts from typical dacitic lava: (a) unresolved plagioclase PI-2 and (b) resorbed plagioclase PI-3. Symbols are the same as in Figure 5.

**Table 2.** Microprobe analyses of the plagioclase phenocrysts from the Kizimen volcano (Kamchatka).

Description	S <sup>a</sup> , μm	Na <sub>2</sub> O	SiO <sub>2</sub>	K <sub>2</sub> O	Al <sub>2</sub> O <sub>3</sub>	CaO	Total	Fe	Ti	Sr	Mg	Ba	An
Pl 1 from enclave KIZ-07/1 (Fig. 5a)													
core	0	1.10 <sup>b</sup>	43.91	0.02	34.56	18.26	98	4330	150	313	295	n.d. <sup>c</sup>	90.1
core	16	1.09	45.29	0.02	35.12	17.83	99	4400	102	507	314	50	89.9
core	33	1.40	45.91	0.02	34.67	17.27	99	3669	84	456	362	n.d.	87.1
core	66	1.18	45.22	0.02	34.77	17.48	99	3747	96	532	320	n.d.	89.0
core	92	1.53	46.38	0.03	34.73	17.26	100	3778	84	634	362	n.d.	86.0
mantle	118	2.54	47.83	0.03	32.92	15.60	99	3109	60	541	392	n.d.	77.1
mantle	125	2.48	48.10	0.07	32.62	15.55	99	3459	120	558	531	71	77.3
mantle	138	1.25	45.47	0.01	34.90	17.56	99	3661	96	524	368	n.d.	88.5
mantle	170	1.59	46.34	0.02	34.20	17.14	99	4159	120	566	482	64	85.5
mantle	207	1.46	46.04	0.03	34.22	17.21	99	4190	102	642	440	n.d.	86.5
mantle	230	1.32	45.94	0.03	34.48	17.58	99	4236	60	566	398	n.d.	87.9
mantle	246	1.77	46.46	0.02	33.93	17.02	99	4462	156	490	482	n.d.	84.0
mantle	252	1.60	46.16	0.03	34.25	17.15	99	4516	132	456	434	n.d.	85.4
mantle	259	2.31	48.00	0.05	33.32	15.69	99	4407	150	608	519	64	78.7
mantle	266	2.22	47.68	0.04	33.13	15.95	99	4827	186	549	501	50	79.7
rim	275	2.91	49.12	0.06	32.24	14.66	99	4485	174	752	501	64	73.3
rim	282	3.62	50.84	0.09	31.04	13.37	99	3980	186	718	464	106	66.7
rim	285	3.64	51.31	0.09	31.13	13.53	100	3980	180	676	476	199	67.0
rim	292	4.59	53.37	0.11	29.61	11.57	99	3257	198	701	332	78	57.8
rim	295	4.49	53.28	0.13	29.94	12.12	100	3700	204	879	386	135	59.4
rim	305	5.92	56.29	0.18	27.69	9.36	99	2829	126	752	211	312	46.2
rim	328	6.94	58.83	0.31	25.47	7.44	99	3879	228	549	229	483	36.5
M <sup>d</sup> , core	351	4.55	53.40	0.11	29.49	11.69	99	3459	198	667	344	99	58.3
M, rim	367	6.16	57.05	0.23	26.70	8.88	99	2923	144	600	241	312	43.7
Pl 1 from enclave KIZ-01/1													
core	7	1.47	46.19	0.03	35.02	17.21	100	3008	n.d.	1436	308	n.d.	92.0
core	33	2.24	48.13	0.05	33.50	15.90	100	2907	n.d.	1808	362	92	87.4
core	43	1.38	46.20	0.03	34.85	17.29	100	3568	84	1301	332	50	92.5
core	63	2.36	48.53	0.05	33.40	15.83	100	3000	n.d.	1402	398	163	86.8
mantle	130	1.63	45.44	0.04	33.33	17.12	98	4524	138	414	669	n.d.	85.1
mantle	150	1.66	46.93	0.03	34.20	17.07	100	4081	132	482	416	n.d.	91.0
mantle	190	1.80	47.09	0.03	34.20	16.85	100	4602	132	431	476	71	90.2
mantle	207	2.09	47.78	0.04	33.75	16.44	100	4151	174	439	482	n.d.	88.5
mantle	227	1.46	46.47	0.03	34.50	17.34	100	4477	108	456	428	99	92.1
mantle	263	1.19	45.88	0.03	35.04	17.73	100	4415	102	431	356	64	93.6
mantle	307	1.25	45.99	0.03	34.82	17.57	100	4547	96	532	368	99	93.2
mantle	320	1.84	47.32	0.04	34.07	16.68	100	4508	108	684	398	n.d.	89.9
rim1 <sup>e</sup>	327	4.12	52.77	0.10	30.60	12.56	100	3801	156	684	350	64	74.8
rim1	333	6.04	57.07	0.21	27.32	9.26	100	3801	174	591	302	199	59.7
rim2	343	1.94	47.42	0.04	33.79	16.47	100	4858	156	482	416	43	89.3
rim2	353	3.14	50.45	0.08	31.79	14.15	100	5278	204	541	482	71	81.5
M, core	363	3.92	52.03	0.09	30.80	12.71	100	3832	126	718	398	92	76.0
M, rim	373	6.01	57.45	0.24	27.26	9.09	100	3335	168	727	247	199	59.2
Pl 2 from dacitic lava KIZ-07 (Fig. 6a)													
core	92	6.14	55.92	0.30	26.54	8.83	98	1702	n.d.	591	109	284	43.5
core	127	6.45	58.37	0.31	26.80	8.36	100	1438	n.d.	667	109	248	41.0
core	196	6.53	58.57	0.29	26.91	8.32	101	1415	n.d.	574	60	227	45.6
core	346	6.01	57.17	0.25	27.51	9.36	100	1477	60	743	96	170	40.6
core	577	6.39	58.28	0.31	26.68	8.47	100	1485	n.d.	591	103	170	41.5
core	612	6.19	58.25	0.31	26.80	8.49	100	1461	60	642	72	149	42.3
core	738	6.23	58.00	0.29	27.15	8.99	101	1516	60	752	78	234	43.6
mantle	773	5.46	56.04	0.21	28.50	10.09	100	1531	n.d.	710	84	192	49.9
mantle	900	6.49	58.34	0.30	26.86	8.51	100	1524	54	718	84	213	41.3
mantle	981	5.05	54.73	0.20	29.28	11.03	100	1733	n.d.	574	90	135	54.0
mantle	1096	6.01	57.91	0.28	27.26	8.93	100	1524	60	558	84	213	44.3
mantle	1154	5.68	56.52	0.23	28.17	9.85	100	1586	n.d.	701	115	185	48.3
mantle	1235	6.32	58.15	0.34	26.76	8.55	100	1508	54	642	115	270	41.9

**Table 2.** (continued)

Description	S <sup>a</sup> , μm	Na <sub>2</sub> O	SiO <sub>2</sub>	K <sub>2</sub> O	Al <sub>2</sub> O <sub>3</sub>	CaO	Total	Fe	Ti	Sr	Mg	Ba	An
mantle	1396	4.11	52.75	0.12	30.76	12.66	100	1663	60	634	103	156	62.6
mantle	1465	6.72	59.10	0.32	26.45	8.05	101	1399	n.d.	634	66	241	39.1
mantle	1592	5.49	56.64	0.25	28.09	9.89	100	1601	n.d.	718	84	185	49.2
mantle	1858	6.06	57.74	0.27	27.20	8.90	100	1531	60	760	90	213	44.1
mantle	1892	5.42	56.00	0.21	28.36	10.25	100	1555	n.d.	532	78	270	50.5
mantle	2065	6.10	57.73	0.31	27.44	9.01	101	1586	60	634	84	248	44.1
mantle	2135	6.29	57.89	0.30	27.16	8.79	100	1726	60	558	90	220	42.8
mantle	2262	5.87	56.48	0.24	28.07	9.75	100	1640	60	743	72	213	47.2
mantle	2342	5.28	55.42	0.20	28.75	10.43	100	1788	66	574	109	206	51.6
mantle	2435	6.31	58.29	0.28	27.20	8.66	101	2169	60	473	96	248	42.4
mantle	2550	5.29	55.47	0.20	28.62	10.36	100	1819	54	558	115	170	51.4
mantle	2665	6.01	57.61	0.28	27.47	9.08	100	1834	n.d.	549	115	170	44.7
mantle	2792	4.92	54.59	0.20	29.44	11.21	100	2130	60	574	139	234	55.1
mantle	3058	5.57	56.24	0.23	28.11	9.89	100	1959	66	600	109	227	48.8
mantle	3242	5.96	57.48	0.28	27.37	9.14	100	1881	n.d.	473	109	192	45.1
mantle	3369	5.70	56.94	0.24	27.83	9.50	100	2091	78	574	115	255	47.2
rim	3370	4.98	54.92	0.20	28.80	11.19	100	3630	138	574	308	149	54.7
rim	3381	4.97	55.08	0.19	28.84	10.99	100	3653	120	549	332	n.d.	54.4
rim	3382	5.04	54.87	0.20	28.86	10.97	100	3599	102	558	308	135	53.9
M1, core	3462	2.38	48.45	0.04	33.49	15.84	100	3840	156	803	295	64	78.4
M1, mantle	3519	4.16	52.89	0.10	30.41	12.59	100	3428	162	693	368	n.d.	62.2
M1, mantle	3577	2.69	49.42	0.06	32.77	15.37	100	4174	138	549	452	n.d.	75.7
M1, rim	3635	4.82	54.55	0.17	29.20	11.28	100	4773	276	566	476	206	55.8
M2, core	3692	3.65	51.39	0.08	31.27	13.49	100	4524	210	651	513	50	66.8
M2, rim	3750	4.69	54.37	0.18	29.26	11.43	100	5402	312	735	488	241	56.8
Pl 2 from dacitic lava KIZ-07													
core	21	5.83	56.38	0.26	27.27	9.40	99	2021	60	583	115	213	46.4
core	75	5.77	56.51	0.22	27.68	9.66	100	1912	60	465	84	241	47.4
core	139	5.74	56.84	0.25	27.77	9.50	100	2060	54	651	127	263	47.1
core	204	5.38	55.99	0.21	28.42	10.17	100	1974	54	667	90	142	50.5
core	268	5.74	56.84	0.24	27.76	9.51	100	1990	60	634	133	284	47.1
core	439	5.89	57.18	0.26	27.57	9.36	100	2083	n.d.	498	133	156	46.0
core	450	5.81	57.28	0.25	27.68	9.38	100	1998	60	456	103	227	46.4
mantle	514	4.56	53.75	0.18	29.72	11.68	100	2223	78	566	96	78	58.0
mantle	525	4.96	54.64	0.19	29.16	11.02	100	2215	84	574	121	185	54.5
mantle	611	4.67	53.87	0.17	29.85	11.65	100	2239	78	507	96	206	57.4
mantle	621	5.65	57.07	0.25	27.81	9.39	100	2052	60	549	109	241	47.2
mantle	686	5.84	56.99	0.24	27.70	9.47	100	1982	54	693	90	220	46.6
mantle	750	4.35	52.77	0.13	30.61	12.48	100	2417	78	532	127	106	60.9
mantle	761	5.30	55.41	0.23	28.58	10.46	100	2573	108	558	362	121	51.5
mantle	782	3.32	50.94	0.10	31.81	13.79	100	2565	84	558	133	57	69.2
mantle	793	3.23	50.87	0.09	31.92	14.10	100	2557	78	659	121	106	70.3
mantle	804	5.82	56.91	0.23	27.85	9.59	100	2005	60	515	109	170	47.0
mantle	814	5.27	55.46	0.21	28.76	10.48	100	2083	60	659	115	234	51.7
mantle	825	4.18	52.71	0.13	30.72	12.52	100	2557	78	524	133	106	61.9
mantle	836	5.03	55.12	0.21	28.70	10.63	100	2394	108	549	181	177	53.2
mantle	846	5.70	56.91	0.24	27.93	9.67	100	2091	66	482	133	170	47.7
mantle	932	5.98	57.05	0.25	27.80	9.30	100	2130	54	566	133	220	45.5
rim1	996	4.43	53.19	0.17	29.95	12.02	100	3762	102	414	344	85	59.4
rim1	1018	5.35	55.75	0.22	28.31	10.49	100	3723	174	642	308	177	51.3
rim2	1039	5.75	56.80	0.25	27.86	9.49	100	2371	66	727	175	177	47.0
rim2	1058	3.76	51.72	0.13	30.87	13.22	100	3078	132	887	163	106	65.5
rim2	1075	2.98	50.16	0.08	32.42	14.57	100	2892	96	490	127	99	72.6
rim2	1093	5.08	54.64	0.20	28.97	11.00	100	3692	138	634	332	291	53.9
M1, core	1125	2.58	49.10	0.05	32.83	15.28	100	4470	186	574	513	n.d.	76.4
M1, rim	1157	5.05	54.89	0.16	28.94	11.07	100	3817	192	701	362	213	54.3
M2, core	1179	4.29	53.55	0.15	29.92	12.12	100	4050	174	718	380	121	60.4
M2, rim	1200	5.10	55.18	0.20	28.69	10.75	100	3716	162	684	302	206	53.2

Table 2. (continued)

Description	S <sup>a</sup> , $\mu\text{m}$	Na <sub>2</sub> O	SiO <sub>2</sub>	K <sub>2</sub> O	Al <sub>2</sub> O <sub>3</sub>	CaO	Total	Fe	Ti	Sr	Mg	Ba	An
Pl 3 from enclave KIZ-07/1 (Fig. 5b)													
core	22	5.27	55.34	0.21	28.53	10.49	100	2013	114	541	133	170	51.7
core	111	6.07	57.02	0.29	27.17	9.07	100	1897	n.d.	659	109	248	44.5
core	211	5.91	56.45	0.23	27.60	9.60	100	1866	n.d.	431	103	234	46.7
core	256	5.57	55.06	0.23	28.28	10.09	99	2060	60	600	96	206	49.3
core	300	5.85	56.58	0.27	27.32	9.35	99	1974	66	659	103	227	46.2
core	378	5.24	54.85	0.20	28.50	10.60	99	2021	54	608	115	206	52.2
core	411	5.95	56.90	0.25	27.25	9.06	99	1936	48	591	103	241	45.0
mantle	467	3.88	51.64	0.12	30.78	12.83	99	2200	102	667	90	85	64.1
mantle	522	4.58	53.18	0.16	29.79	11.68	99	2114	60	566	115	99	58.0
mantle	556	5.00	54.55	0.18	29.04	10.78	100	1982	78	651	115	248	53.8
mantle	589	3.61	50.99	0.12	31.20	13.27	99	2332	66	819	121	142	66.6
mantle	611	3.96	51.57	0.14	30.85	12.82	99	2223	54	600	139	149	63.6
mantle	700	6.28	57.46	0.29	26.69	8.59	99	1904	78	363	121	234	42.4
mantle	733	4.95	54.60	0.20	28.92	10.91	100	2107	60	752	109	248	54.3
mantle	800	6.00	56.85	0.27	27.32	9.10	100	1912	54	524	115	206	44.9
mantle	900	6.10	57.05	0.26	27.43	9.05	100	1904	60	718	96	227	44.4
mantle	1011	5.74	56.43	0.27	27.52	9.41	99	1866	54	718	109	206	46.8
mantle	1044	6.24	57.10	0.27	27.05	8.94	100	1858	60	498	115	227	43.5
mantle	1133	6.04	57.25	0.29	26.95	8.67	99	2005	54	659	90	305	43.4
mantle	1167	3.94	51.42	0.13	30.88	13.07	99	2379	108	659	121	135	64.2
mantle	1222	5.66	56.59	0.25	27.73	9.46	100	2060	60	482	127	270	47.3
mantle	1267	5.55	55.72	0.23	28.08	9.94	100	2262	60	718	103	241	49.1
R <sup>f</sup>	1333	3.20	51.52	0.24	30.75	13.35	99	4843	246	617	416	135	68.7
R	1367	3.27	50.43	0.07	31.81	14.14	100	3957	156	507	458	85	70.2
rim1	1422	4.69	53.63	0.13	29.81	11.56	100	3327	180	507	295	57	57.2
rim1	1467	5.62	55.69	0.16	28.04	9.87	99	2930	102	473	235	213	48.8
rim2	1511	3.35	50.36	0.09	31.68	13.98	99	3941	132	566	464	85	69.4
rim2	1541	4.02	52.29	0.09	30.44	12.69	100	3653	204	710	380	149	63.2
rim2	1570	4.94	54.44	0.13	29.13	11.02	100	3148	162	710	283	106	54.8
rim2	1600	5.60	56.68	0.17	28.07	9.74	100	3039	132	667	235	156	48.5
M, core	1622	3.39	50.62	0.08	31.41	14.10	100	4198	180	710	513	92	69.4
M, rim	1656	5.50	55.24	0.16	28.78	10.55	100	2604	162	743	235	78	51.0
Pl 3 from dacitic lava KIZ-07 (Fig. 6b)													
core	0	5.92	56.94	0.26	27.90	9.63	101	1850	n.d.	600	103	199	46.6
mantle	91	5.52	56.05	0.23	28.37	10.16	100	1842	78	625	121	163	49.8
mantle	121	6.12	57.89	0.30	27.08	8.79	100	1850	60	608	103	234	43.4
mantle	145	5.85	56.61	0.25	28.05	9.74	100	1858	72	659	109	234	47.2
mantle	170	6.43	58.55	0.32	26.67	8.48	100	1827	60	769	103	270	41.4
mantle	188	5.94	57.81	0.28	27.55	9.01	101	1873	n.d.	456	103	305	44.9
mantle	212	5.77	56.40	0.22	28.25	9.96	101	2037	n.d.	634	115	291	48.2
mantle	224	5.72	56.33	0.22	28.28	9.90	100	2013	n.d.	676	115	263	48.3
mantle	236	5.98	57.20	0.25	27.69	9.26	100	1873	102	803	96	305	45.4
mantle	255	5.47	56.68	0.24	28.02	9.69	100	1967	90	684	90	206	48.7
mantle	321	6.15	57.94	0.28	27.21	8.76	100	2044	60	524	96	312	43.3
mantle	358	5.46	55.60	0.22	28.50	10.27	100	2107	72	574	115	263	50.3
mantle	400	6.09	57.59	0.29	27.23	8.99	100	1881	60	583	103	213	44.1
mantle	467	4.93	54.68	0.18	29.47	11.20	100	2278	72	659	133	234	55.1
mantle	491	5.75	56.68	0.23	28.02	9.86	101	2231	78	541	109	213	48.0
mantle	521	5.95	56.89	0.25	27.76	9.62	100	2122	108	625	109	255	46.5
mantle	576	5.89	56.92	0.27	27.79	9.60	100	2044	96	583	127	206	46.7
R	679	2.80	49.65	0.15	31.79	14.31	99	4998	216	507	470	64	73.1
rim	721	2.52	48.81	0.06	32.71	15.41	100	4578	186	583	549	64	76.9
rim	727	2.58	48.99	0.07	32.74	15.41	100	4485	132	591	494	71	76.5
rim	733	3.52	51.08	0.09	30.97	13.61	99	4415	162	507	458	50	67.7
rim	745	4.51	53.00	0.14	29.88	12.19	100	4205	192	507	350	128	59.4
rim	752	3.84	52.03	0.11	30.68	13.15	100	4034	162	515	398	43	65.0
rim	758	5.06	55.16	0.19	28.57	10.88	100	3879	186	566	344	149	53.7

**Table 2.** (continued)

Description	S <sup>a</sup> , $\mu\text{m}$	Na <sub>2</sub> O	SiO <sub>2</sub>	K <sub>2</sub> O	Al <sub>2</sub> O <sub>3</sub>	CaO	Total	Fe	Ti	Sr	Mg	Ba	An
rim	764	5.05	55.03	0.18	28.64	10.91	100	4485	216	574	308	156	53.8
M, core	818	3.08	49.91	0.08	31.84	14.35	99	4749	180	490	537	43	71.7
M, rim	848	3.88	52.01	0.13	30.41	12.80	99	5200	306	566	555	99	64.1

<sup>a</sup> S - distance from the phenocryst core in microns.

<sup>b</sup> Major elements (Na<sub>2</sub>O, SiO<sub>2</sub>, K<sub>2</sub>O, Al<sub>2</sub>O<sub>3</sub> and CaO) are given in wt. %, minor and trace elements (Fe, Ti, Sr, Mg and Ba) - in ppm.

<sup>c</sup> n.d. - not detected.

<sup>d</sup> M - microlite. One or two plagioclase microlites were analysed near by each plagioclase phenocrysts – M1 and M2, respectively.

<sup>e</sup> Outer rims in some grains were measured at different edges of crystal – rim1 and rim2, respectively.

<sup>f</sup> R – resorption zone.

## 5. DISCUSSION

Kizimen rocks reveal many features commonly attributed to magma mixing: a) presence of olivine and orthopyroxene of constant composition (Fo<sub>79-72</sub> and En<sub>63-65</sub>Wo<sub>1-2</sub>, respectively) in all rocks, independent of melt composition; b) coexistence of olivine and quartz; and c) coexistence of plagioclases with high-An core and low-An rims and with low-An cores at high-An rims. Mixing between silicic and mafic end-members is consistent with the observed linear trends on all two-component diagrams for this volcano (e.g. Figure 3). The abundance and size of enclaves in many lava flows as well as numerous banded lavas suggest that the mixing processes play an unusually profound role in magma genesis at Kizimen volcano.

If all Kizimen rocks from dacitic host lavas to mafic enclaves are indeed hybrids, the temporal trend for mafic enclaves on the SiO<sub>2</sub>-K<sub>2</sub>O diagram either suggests that magma chamber recharge is getting more mafic or that the proportion of the mafic end-member increases with time (Figure 3).

From Sr and Nd isotope data, which are very similar in all rocks and close to MORB values, there is not evidence for any crustal contamination.

Trace element patterns of variably differentiated magmas, which crystallized from the same parent should have sub-parallel patterns, where more evolved rocks are more enriched in all incompatible elements. This is valid however, only as long as olivine, clino- and orthopyroxene, plagioclase, and spinel (or magnetite) are the only crystallizing phases. This is because all of them have low partition coefficients for incompatible trace elements. Theoretically, the observed cross-over patterns could be explained as a result of magmas coming from different mantle sources. However, cross-over patterns on spider diagrams for the rocks of Bakening volcano were modeled by *Dorendorf et al.* [2000b] as depletion of the dacitic magma in HREE by extensive hornblende fractionation from basaltic melt. We suggest that basalts and dacites of Kizimen volcano were also affected by a strong amphibole signature and thus originated

from similar mantle melts. This is reasonable, because all lavas at Kizimen, including the mafic varieties, are rich in amphibole.

According to petrographical and geochemical data (Fo<sub>72-78</sub> olivine, Mg# 41 to 50 of whole rocks, abundance of low-An plagioclase, and low Cr and Ni concentrations in whole rocks), mafic enclaves are already fractionated compared to primary mantle melts and are contaminated by incorporation of more evolved material, which may or may not be derived directly from the host. Similarly, the presence of high-An plagioclase and traces of olivine in Kizimen dacites suggest that the host lavas are contaminated by mafic debris from enclaves. Thus, both host and enclaves are hybrids formed by mixing of more extreme end-members.

Over the last decade it was shown that trace elements in zoned minerals are a useful tool to identify mixing end-members [e.g. *Brophy et al.*, 1996; *Davidson and Tepley*, 1997; *Ginibre et al.*, 2002a, 2002b]. Our discussion of mixing end-members and mixing events is based on trace element variations in plagioclase. The Mg and Fe content in plagioclase phenocrysts shows two trends when plotted against An (Figure 7). Cores of Pl-1 phenocrysts from mafic enclaves are highest in An (An<sub>75</sub>-An<sub>94</sub>), Mg (300–550 ppm) and Fe (2900–4600 ppm) compared to all other crystals. These high-An, high-Mg, and high-Fe plagioclases probably have grown in a relatively mafic source. Rare crystals of “mafic” plagioclases reveal some resorption in the core (Figure 5a), but the mantle zone and outer rim are never resorbed. This observation suggests that Pl-1 mainly crystallized from a relatively high-temperature melt and was not dissolved during the later mixing events before eruptions. Experimental values of  $Kd_{Mg}$  in plagioclase vary between 0.025 and 0.05 [e.g. *Bindeman et al.* 1998]. Using  $Kd_{Mg}$  of 0.035, the calculated MgO concentration in the most mafic melt is  $3.17 \pm 0.5$  wt%, which is of the same order as MgO concentration in whole rock composition of mafic enclaves (Table 1, samples KIZ-01/1; KIZ-07/1; KIZ-24/1). High-An plagioclases were found in all enclaves but only traces of Pl-1 were found in host lavas. Therefore, these feldspars are considered phenocrysts from a magma close to the mafic end-member.

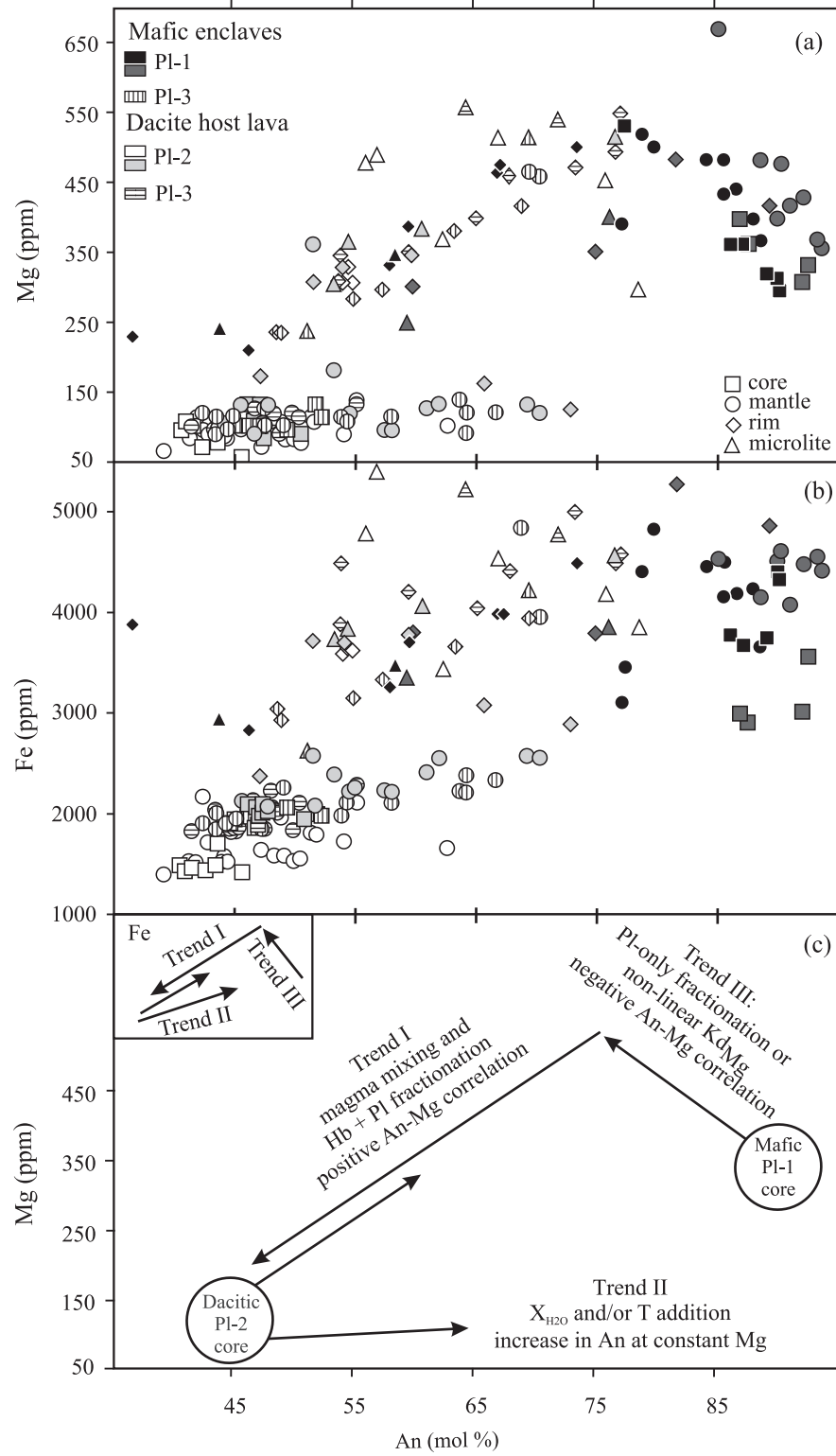


**Figure 7.** Mg (a) and Fe (b) variations with An-content in Kizimen plagioclase: squares – cores, circles – middle zones, diamonds – rims, triangles - microlites; (c) schematic evolution of the crystals. Arrows show direction of evolutionary trends from core to rim. See text for further explanation and discussion of the trends.

In contrast, the cores of Pl-2 from the host dacitic lava are lowest in An ( $An_{40}$ - $An_{50}$ ), Mg (50–100 ppm), and Fe (1500–2000 ppm). These low-An plagioclases probably formed in the evolved end-member, but are now found in both, the mafic enclave and the host dacite.

The sodic and low-Mg (and low-Fe) cores of the plagioclases Pl-3 from both mafic enclaves and host lavas are similar to Pl-2 from the host lavas (Figures 5b, 6, 7). Similarity of compositions of Pl-2 and Pl-3 suggests that all these crystals formed in the same relatively evolved melt.

Mantle zones and rims of plagioclases from enclave and lava show different histories. Pl-1 from enclaves displays a typical fractionation trend (Trend I in Figure 7c) with decreasing An and Mg content from core to rim. Mantle zones and rims from Pl-2 of the host lavas show two different trends. One falls on the differentiation trend I (correlated, outward decreasing An, Mg, and Fe). The second trend II, which is also represented in mantles and rims of sodic plagioclase (Pl-2 and all grains Pl-3) is characterized by increasing in An from core to rim at nearly constant Mg content and slightly increasing Fe content. Apparently, these two separate trends could be explained by two different processes. Trend I likely represents a differentiation trend overprinted by repeated mixing events between different members of the differentiation series. This is consistent with the reversals in An between core and rim (Figure 7c). Dissolution features near the rims of sodic plagioclases are then explained by mixing between more extreme melt compositions: low-temperature dacitic magma and high-temperature basaltic melt. This is consistent with the observation that this late-grown An-rich plagioclase rim is also characterized by high concentrations of Mg and low of Ba and Sr contents (for example, point 18, Figure 6b). Microlites then grew from the hybrid melt with compositions similar to the rims of these phenocrysts.

Crystals which grew from the basaltic high-temperature melt in mafic enclaves (Pl-1, Figure 5a) before incorporation of enclaves in the host dacite did not subsequently dissolve significantly. The abrupt change in chemical composition at their late-grown rims relative to their inner zones (decreasing An, Mg and Fe and increasing Ba and Sr, Figure 5a) also suggests a magma mixing processes just before or during eruption. The fact that these crystals are rather homogeneous in their cores with respect to An and minor and trace elements (Figure 5a) argues that they record a quiet growth environment in the mafic end-member magma before mixing.

Cores of the most sodic low-An plagioclases fall on the continuation of trend I (Figure 7) and are probably the result of mixing late in the differentiation process.

Trend II is more difficult to explain. It is characterized by repetitive cycles of increasing and decreasing An con-

tent, however, without correlated changes in Mg (or with slight increase in Fe) content. This observation excludes simple mixing of variably differentiated magmas to explain resorption and An variations (Figure 7b). It was shown that  $Kd_{Mg}$  in plagioclase varies within a very narrow range, and correlates weakly with T [Longhi *et al.*, 1976] and An content [Bindeman *et al.* 1998]. In the presence of hornblende and Opx crystallization and decreasing Mg (and Fe) in the melt, the effect of variable An on Mg (and Fe) partitioning is inconsistent with the observed constant Mg concentrations [see Ginibre *et al.*, 2002b for a more detailed discussion of the An-dependent trace element partitioning in plagioclase]. This trend could then be caused by either increasing temperature and/or increasing water content in the melt. Low An content and concentrations of magnesium (and Fe) in these plagioclases indicate that the melt was certainly not more mafic. At increased temperature, the sodic plagioclase would dissolve in hotter melt and the new more An-rich plagioclase starts to grow. Consequently, variable An at constant Mg could reflect a thermal rather than a compositional disturbance of the host melt. An increase in temperature aided by incomplete mixing when heat from a high-temperature basaltic/basaltic-andesite magma is transported into the low-temperature host dacite by thermal conduction could occur without effect on trace elements in the melt and in crystallized plagioclase.

Alternatively, variable An at constant Mg may be expected when the water content in the melt increases. In this case, a single plagioclase phenocryst may have moved into (and out of) a water-rich boundary layer of the magma chamber [Ginibre *et al.*, 2002a]. However such repeated movements of phenocrysts are less likely in the highly viscous dacite melt and therefore we favor the first scenario of “thermal” mixing.

Finally, an unusual behavior of Mg vs. An (less so for Fe) was found in Pl-1 grains from mafic enclaves: increasing Mg at decreasing An from cores to mantle (Trend III in Figure 7). Such Mg (and Fe) behavior was only observed in the highest-An zones of the crystals ( $An_{75-95}$ ). Because trend for Mg are more pronounced compare to Fe (Figures 7a and 7b), our future discussion would be based on Mg content in plagioclases. Several scenarios are considered to explain this trend:

(1) The continuous replenishment of the magma chamber by a high-Mg melt. The existence of sieved textures in the core of some Pl-1 (Figure 5a) could suggest magma mixing events in the early stages of the plagioclase crystallization. However, negative correlations between An and Mg (and Fe) in plagioclase Pl-1 is observed along the core and mantle zone of the crystal. Also, continuous recharge would be expected to result in resorption and subsequent regrowth, which is not

observed in Pl-1 mantle. On the basis of these arguments, we rule out an origin from highly mafic magmas.

(2) Considering the linear relation between An and Mg partitioning in plagioclase [Bindeman *et al.*, 1998], the zoning could indicate an early phase of crystallization where plagioclase was the only phase. As a result, prior to the onset of olivine and pyroxene fractionation, the An content could decrease while Mg (and Fe) increases. This explanation was tested by a fractional crystallization model of a melt similar in composition to the most mafic end-member enclave (represented by a high-Al basalt KIZ-01/1, Table 1) based on the COMAGMAT program at 1% of H<sub>2</sub>O and NNO buffer. The pressure in the model (125 MPa) was taken from petrological experiments [Churikova *et al.*, 2001b; B. Browne, personal comm.], assuming that the magma chamber was not at a significantly different depth during melt evolution and later mixing.

As shown in Figure 8, the modeled compositions fall close to the observed magma compositions at Kizimen and are consistent with decreasing An in the plagioclase coupled with increasing Mg and Fe in the melt (Figure 8a, b, f) very early in the crystallization sequence. Thus, this model is consistent with Trend III. Observed olivine and pyroxene compositions are also reproduced well in the model: olivines and clinopyroxenes in mafic enclaves are Fo<sub>79-75</sub> and En<sub>44</sub>Fs<sub>16</sub>Wo<sub>40</sub> [see also Trusov & Pletchov, 2005], and modeled compositions are Fo<sub>78,5-76</sub> and En<sub>43-46</sub>Fs<sub>12-17</sub>Wo<sub>40-42</sub>, respectively.

However, the most calcic plagioclase calculated in the model is at An<sub>84-85</sub>, whereas inner parts of Pl-1 in basalt and basaltic andesite enclaves show values up to An<sub>93</sub>. We would argue that this deviation between modeled and observed plagioclase compositions could be a result of the parameters chosen for the model, which may not be completely appropriate but cannot be better constrained. According to our calculations, Trend III (i.e. increasing Mg and Fe with decreasing An) could therefore be controlled by melt composition and Pl-only fractionation in the first stages of high-Al melt evolution.

We do not imply, however, that this melt was a primary magma. Low MgO (4–5%), Ni (less than 2 ppm), Cr (11–20 ppm) and relatively high K<sub>2</sub>O (0,9%) suggest that all enclaves represent already fractionated compositions. The existence of resorbed cores inside of some grains of Pl-1 and the presence of numerous fine-grained basaltic inclusions (enclaves within enclaves) inside the mafic enclaves (Figure 2b) also suggest that the enclave's magma was itself affected by magma mixing events. The crystallization P-T conditions where plagioclase would crystallize first at suppressed Ol and Cpx crystallization are very limited, and according to our model would be possible in subsurface conditions from 1 to 3 Kbar (about 10 km). We believe that such scenario

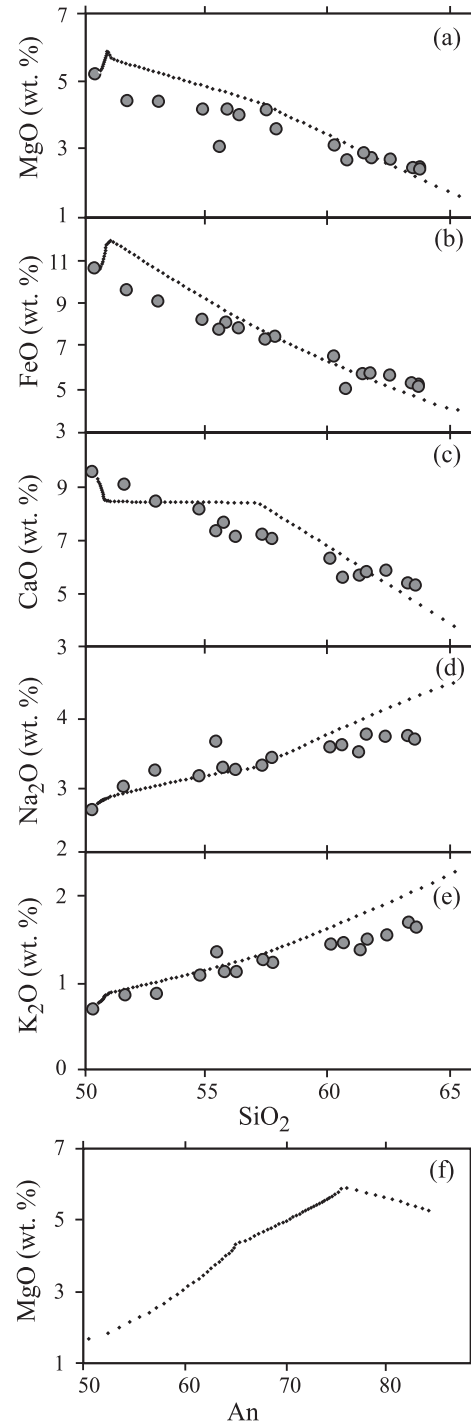


**Figure 8.** Model calculations (dotted line) of the fractional crystallization of basaltic magma from the Kizimen volcano (sample KIZ-96-01/1) in comparison with observed whole rock compositions (gray circles). Calculations were conducted using COMAGMAT program [Ariskin *et al.*, 1993] for P=125Mpa, NNO buffer and H<sub>2</sub>O=1%. Due to Pl fractionation during the first stage of crystallization the residual melt is enriched in MgO.

is possible at Kizimen volcano, but other alternatives are possible.

(3) An other explanation of the trend III is non-linear behavior of  $Kd_{Mg}$  in high-An plagioclases.

Sato [1989] noted that, due to kinetic disequilibrium, the distribution coefficients determined by the experiments may not represent the true equilibrium values and that as a result partitioning in experiments are significantly different from natural systems.

Experimentally determined  $Kd_{Mg}$  in plagioclase varies in a narrow range and is expected to be linear and almost independent from melt composition [e.g. Bindeman *et al.*, 1998]. In this case the positive correlation of An and Mg in plagioclases would be expected. In fact, positive correlation between An and Mg (and Fe) was observed for relatively sodic plagioclases from the Kizimen volcano (Figure 7c, Trend I). However, at  $An_{75-95}$  we clearly observe the negative correlation between An and Mg in plagioclases (Figure 7c, Trend III). From our point of view, this may testify to non-linear behavior of  $Kd_{Mg}$  (and  $Kd_{Fe}$ ) in high-An plagioclases. We have a reason to claim that such participation of Mg (and Fe) in high-An plagioclases could be found not only at the complex Kizimen volcano, but also in more primitive systems.

McNeill and Danyushevsky [1996] studied the melt inclusions in minerals from MORB basalts from the Costa Rica Rift (Borehole 896A) where Ol, Cpx and Sp were first crys-

tallized phases. According to their data An in plagioclases and MgO and FeO in the equilibrium melts have a positive correlations (Figures 9a, b drawn using data from Tables 3, 7 of McNeill and Danyushevsky, 1996). However, we could observe the trends of negative correlations An with MgO and FeO in all Ca-rich ( $An_{83-95}$ ) plagioclases (Figure 9c, d, data from Table 3, McNeill and Danyushevsky, 1996).

We suggest that negative correlations between An and Mg (less to Fe) in high-An plagioclases at Kizimen could indeed be a function of non-linear behavior of  $Kd_{Mg}$ , for example, due to non-equilibrium processes in the Pl-melt system and not directly controlled by melt composition. To our knowledge, this effect has not been documented before and requires additional experimental work for an understanding of  $Kd_{Mg}$  and  $Kd_{Fe}$  in high-An plagioclases.

Figure 10 shows a schematic model of the magma system below Kizimen volcano, which summarizes our interpretations. Mafic magma (with high-An Pl-1) is introduced to the dacitic magma chamber (with sodic Pl-2) bringing the two magmas in direct contact. This process forms hybrids where two contrasting domains, the enclaves and host lava, show the effects of both chemical and physical mixing (Figure 2c). Pl-2 of bearing dacite, engulfed in mafic magma would be exposed to high temperature, resulting in plagioclase dissolution and transition of Pl-2 in Pl-3. The newly hybrid melt around this plagioclase would be more mafic, resulting in more calcic rims on the resorbed sodic mantle zones of

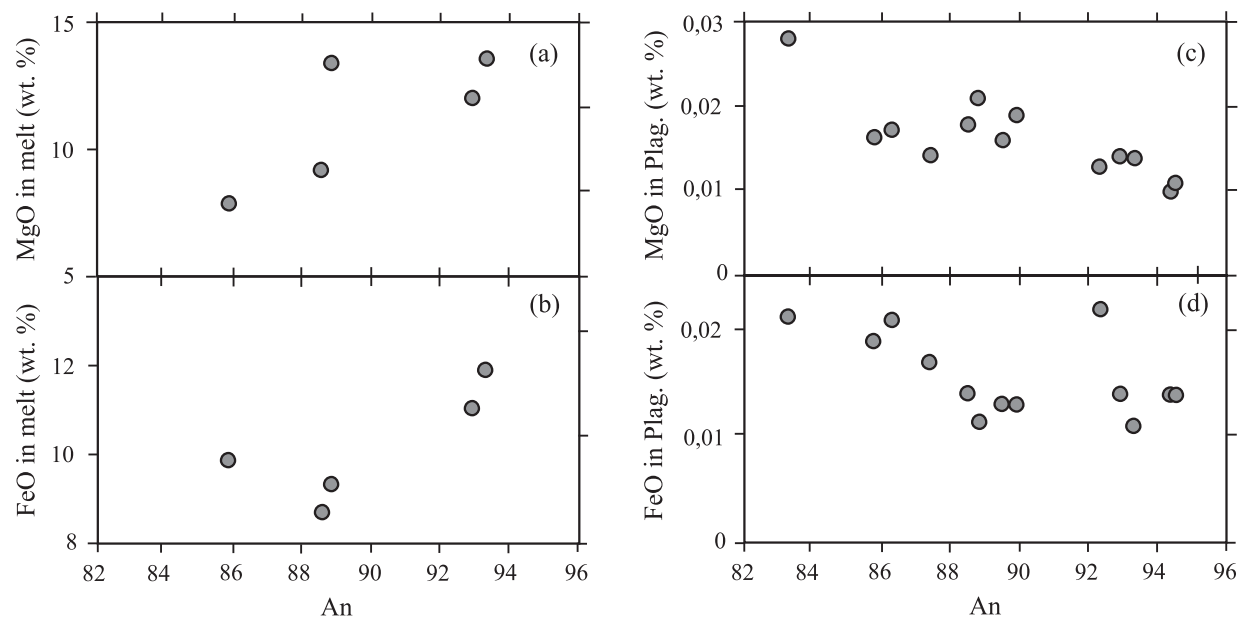


**Figure 9.** MgO and FeO in melt inclusions versus An component of host plagioclase (a, b) and MgO and FeO concentrations in plagioclase versus An component (c, d) from MORB basalts of the Costa Rica Rift (Borehole 896A; data from McNeill and Danyushevsky, 1996, Tables 3, 7).

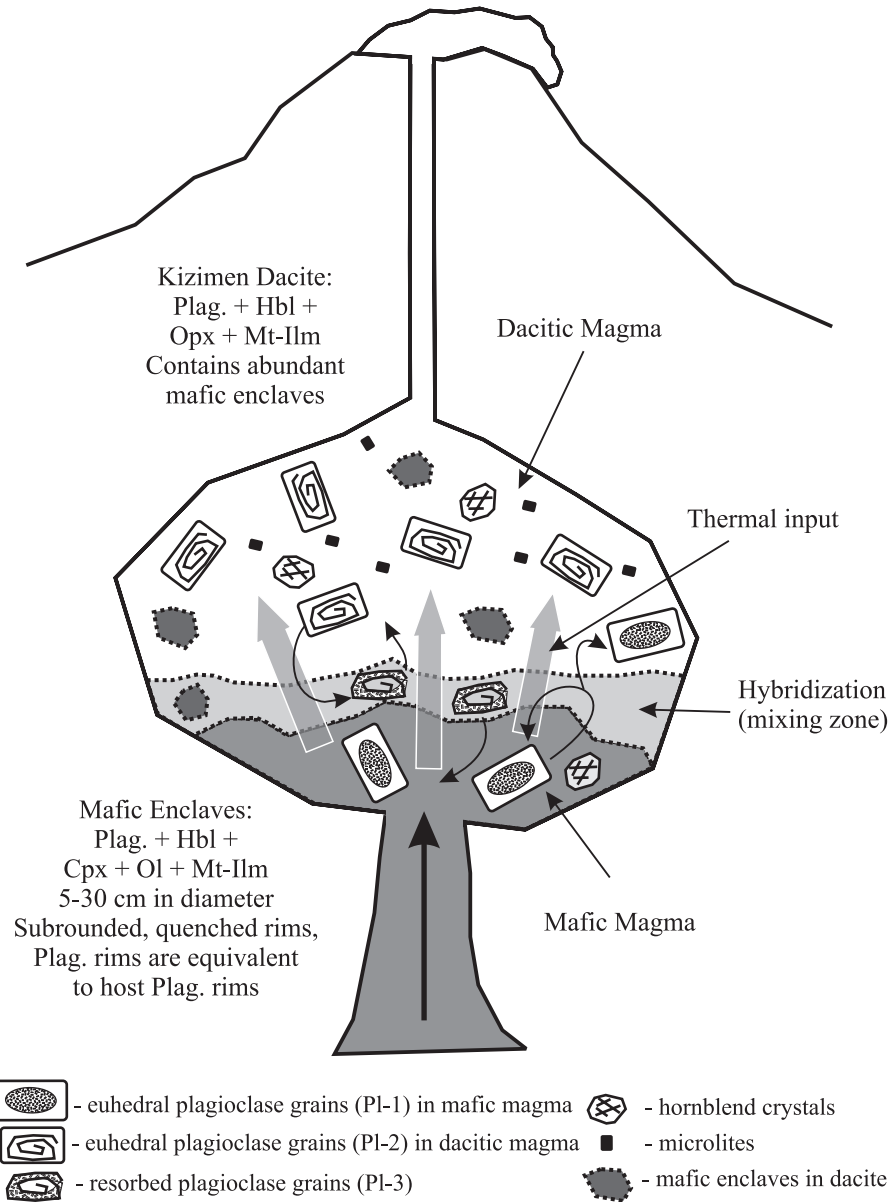


**Figure 10.** Schematic cartoon illustrating different processes in magma chamber of the Kizimen volcano. Due to a recharge of the basaltic magma inside dacitic magma chamber interactions between two melts are complex. Melts and their crystals could be changed by direct physical and chemical mixing within the mixing zone forming hybrid magma and streaky lavas or by thermal conduction only. Mafic plagioclase grains from basalt would be not significantly influenced by these processes while acid plagioclases would dissolve at higher temperature conditions and overgrow by new rims from surrounding hybrid and/or overheated melts. The movement of the plagioclase crystals are shown by arrows. More discussion see in text.

PI-3 (e.g. PI-3 and trend I on Figure 7). Some PI-3 is returned to the host dacite through mechanical dispersion of mixing products, while some remains as phenocrysts in enclaves.

Mafic PI-1 from basalt that was entrained in the hybrid zone was not affected by the low-temperature dacite melt and

was not resorbed. However it will be overgrown by a more Ab-rich rim precipitated from the new hybrid melt. Such plagioclases are rare in host lava. But we did observe them in significant quantities in the enclaves, which are hybridized mafic magma.

The recharge and mixing process was not sufficiently effective so as to involve the entire magma volume and thus full homogenization in the magma chamber is not achieved. Some portions of dacitic magma may not have been directly involved in the chemical hybridization process, but were nevertheless subjected to heat from recharge. At increased temperatures, the rims of sodic Pl-2 recrystallized to more An-rich composition, forming trend II on Figure 7.

We speculate that episodic rise of basaltic recharge is particularly frequent (and thus causes a high proportion of mafic enclaves) in an extensional tectonic regime and is sustaining a dynamic and poorly mixed magma body at shallow depth below Kizimen. Interactions between magmas at Kizimen are complex, and apparently share many similarities with interactions at Unzen [Eichelberger *et al.*, 2006].

## 6. CONCLUSIONS

Based on textural evidence from plagioclase growth zones and major, minor and trace element contents, we conclude that:

- 1) All rocks of Kizimen volcano, including mafic enclaves, are hybrids and represent mixture of mafic and acid end-members in different proportions. These end-members are likely to be derived melts from the same parental melt by crystal fractionation including amphibole.
- 2) The unusual negative correlation of Mg with An in high-An plagioclase can be explained by fractional crystallization of the high-Al basalt with Pl-only fractionation or by non-linear behavior of  $Kd_{Mg}$  in Pl-melt system.
- 3) Incomplete mixing maintains the physical identity of distinct, though somewhat hybridized, end-members. While (incomplete) chemical mixing is abundant, we also observe evidence for the transport of heat (or increased water content) only in the variation of An content in plagioclase at constant trace element concentrations.
- 4) The trend within mafic enclaves toward more mafic compositions with time at Kizimen indicates that generation (by fractional crystallization) of the evolved dacite is not keeping pace with mafic recharge and outputs are likely directly triggered by inputs.

*Acknowledgments.* Martin Streck, Pavel Izbekov and Andrey Babansky are thanked for their detailed and constructive comments on an earlier version of this manuscript. Brandon Browne and Boris Gordeichik helped a lot with graphics preparation. This work was possible with a support of grant DFG #Wo362/15-1+2 to G.W., DFG-RFBR grant #00-0504000 to T.C. and G.W., projects of “Program 13” of RAS Presidium, Ministry of Industry and Science projects #43.700.11.0005, 43.043.11.1606 and State Contract with Federal Agency of Science and Innovations’ Department of Survey and New Technologies Development #01.700.12.0028 to T.C.

## 7. REFERENCES

- Allégre, C. J., A. Provost, and C. Jaupart, Oscillatory zoning: a pathological case of crystal growth, *Nature*, 294, 223–228, 1981.
- Ariskin, A. A., G. S. Barmina, M. Ya. Frenkel, and R. L. Nielsen, COMAGMAT: a Fortran program to model magma differentiation processes, *Computers and Geosciences*, 19, 1155–1170, 1993.
- Bindeman, I. N., A. M. Davis, and M. J. Drake, Ion microprobe study of plagioclase—basalt partition experiments at natural concentration level of trace elements, *Cosmochim Geochim Acta* 62, 1175–1193, 1998.
- Brophy, J. G., M. J. Dorais, J. Donnelly-Nolan, and B. Singer, Plagioclase zonation in hornblende gabbro inclusions from Little Glass Mountain, Medicine Lake volcano, California: implications for fractionation mechanisms and the formation of composition gaps, *Contrib Mineral Petrol*, 126, 121–136, 1996.
- Browne, B. L., J. C. Eichelberger, L. Patino, T.A. Vogel, J. Dehn, K. Uto, and H. Hoshizumi, Generation of porphyritic and equigranular mafic enclaves during magma recharge events at Unzen Volcano, Japan, *J. Petrol*, 47, 301–328, 2006.
- Churikova, T. G., and S. Yu. Sokolov, The magmatic evolution of Ploskie Sopky volcano, Kamchatka (analyses of Sr isotopic geochemistry), *Geochemistry*, 10, 1439–1448, 1993.
- Churikova, T., F. Dorendorf, and G. Wörner, Sources and Fluids in the Mantle Wedge Below Kamchatka, Evidence from Across-Arc Geochemical Variation, *J. of Petrology*, 42 (8), 1567–1593, 2001a.
- Churikova, T., B. Ivanov, J. Eichelberger, S. Trusov, J. Gardner, A. Belousov, B. Browne, P. Izbekov, and G. Wörner, Kizimen Volcano: An Unzen-like Magma System in Kamchatka, *AGU Fall Meeting, EOS*, 82 (47), F1381, 2001b.
- Davidson, J. P., F. J. Tepley, Recharge in volcanic system: evidence from isotope profiles of phenocrysts, *Science*, 275, 826–829, 1997.
- Drake, M. J., and D. F. Weill, Partition of Sr, Ba, Eu<sup>2+</sup>, Eu<sup>3+</sup> and other REE between plagioclase feldspar and magmatic liquid: an experimental study, *Geochim Cosmochim Acta*, 39, 689–712, 1975.
- Dorendorf, F., U. Wiechert, and G. Wörner, Hydrated sub-arc mantle: a source for the Kluchevskoy volcano, Kamchatka Russia, *Earth and Planetary Science Letters*, 175, 69–86, 2000a.
- Dorendorf, F., T. Churikova, A. Koloskov, and G. Wörner, Late Pleistocene to Holocene activity at Bakening volcano and surrounding monogenetic centers (Kamchatka): volcanic geology and geochemical evolution, *Journal of Volcanology and Geothermal Research*, 104, 131–151, 2000b.
- Eichelberger, J. C., P. Izbekov, and B. Browne, Bulk chemical trends at arc volcanoes are not liquid lines of descent, *Lithos*, 87, 135–154, 2006.
- Ginibre, C., A. Kronz, and G. Wörner, High-resolution quantitative imaging of plagioclase composition using accumulated back-scattered electron images: new constraints on oscillatory zoning, *Contrib Mineral Petrol*, 142, 436–448, 2002a.
- Ginibre, C., G. Wörner, and A. Kronz, Minor- and trace-element zoning in plagioclase: implications for magma chamber processes at Parinacota volcano, northern Chile, *Contrib Mineral Petrol*, 143, 300–315, 2002b.
- Grove, T. L., M. B. Baker, and R. J. Kinzler, Coupled CaAl-NaSi diffusion in plagioclase feldspar: Experiments and application

- to cooling rate speedometry, *Geochim Cosmochim Acta*, 58, 2113–2121, 1981.
- Longhi, J., D. Walker, and J. F. Hays, Fe and Mg in plagioclase. *In: Proc 7th Lunar Sci Conf*, 1281–1300, 1976.
- Marsh, B. D., Magma chambers, *Annu Rev Earth Planet Sci*, 17, 439–474, 1989.
- Melekestsev, I. V., V. V. Ponomareva, and O.N. Volynets, Volcano Kizimen (Kamchatka)—future Sent-Helens, *Volcanology and seismology*, 4, 3–31, 1992.
- McNeill, A. W., and L. V. Danyushevsky, Composition and crystallization temperatures of primary melts from hole 896A basalts: evidence from melt inclusion studies. *In: Proc. ODP, Scientific results*, 148, 21–35, 1996.
- Nakada, S., and Y. Motomura, Petrology of the 1991–1995 eruption at Unzen; effusion pulsation and groundmass crystallization, *J. Volcanol. Geotherm. Res.* 89, 173–196, 1999.
- Sato, H., Mg-Fe partitioning between plagioclase and liquid in basalts of Hole 504B, ODP Leg 111: A study of melting at 1 atm, *Proc. Ocean Drilling Program, Sci. Results*, 111, 17–26, 1989.
- Sun, S. S., and W. F. McDonough, Chemical and isotopic systematics of oceanic basalts; implications for mantle composition and processes, *in: Saunders, A.D. & Norry, M.J. (eds) Magmatism in the ocean basins. Geological Society Special Publications. London: Geological Society of London*, 313–345, 1989.
- Tepley, F. J. III, J. P. Davidson, R. I. Tilling, and J. G. Arth, Magma mixing, recharge and eruption histories recorded in plagioclase phenocrysts from El Chichon Volcano, Mexico, *J Petrol*, 41, 1397–1411, 2000.
- Todt, W., R. A. Cliff, A. Hanser, and A.W. Hofmann,  $^{202}\text{Pb}$ - $^{205}\text{Pb}$  spike for Pb isotope analysis. *Terra Cognita*, 4, 209, 1984.
- Trusov, S. V., and P. Yu. Pletchov, Formation of antidromic series of the Kizimen volcano (Kamchatka). *International petrographical Meeting „Petrography of XXI century“*, June, Apatiti, 2005 (in Russian).

---

Alaska Volcano Observatory, Geophysical Institute, University of Alaska Fairbanks, USA

Geowissenschaftliches Zentrum Göttingen, Universität Göttingen, Germany

Institute of Volcanology and Seismology, Piip Avenue, 9, Petropavlovsk-Kamchatsky, 683006, Russia

